

Optimal compressive multiphoton imaging at depth using single-pixel detection

PHILIP WIJESINGHE¹, ADRIÀ ESCOBET-MONTALBÁN¹, MINGZHOU CHEN¹, PETER R T MUNRO², AND KISHAN DHOLAKIA¹

¹SUPA, School of Physics and Astronomy, University of St Andrews, North Haugh, St Andrews, KY16 9SS, UK

²Department of Medical Physics and Biomedical Engineering, University College London, Gower Street, London WC1E 6BT, UK

Compiled August 9, 2019

Compressive sensing can overcome the Nyquist criterion and record images with a fraction of the usual number of measurements required. However, conventional measurement bases are susceptible to diffraction and scattering, prevalent in high-resolution microscopy. Here, we explore the random Morlet basis as an optimal set for compressive multiphoton imaging, based on its ability to minimise the space-frequency uncertainty. We implement this approach for the newly developed method of wide-field multiphoton microscopy with single-pixel detection (TRAFIX), which allows imaging through turbid media without correction. The Morlet basis promises a route for rapid acquisition with lower photodamage.

© 2019 Optical Society of America

<http://dx.doi.org/10.1364/ao.XX.XXXXXX>

Optical imaging at depth has gained a strong impetus in the past decade as it allows access to rich and intricate molecular information in three dimensions, even within living animals. This is now a burgeoning need in several fields, including neuroscience [1] and histopathology [2]. Researchers are particularly drawn to multiphoton microscopy (MPM), specifically two-photon and latterly three-photon modes, which allow deeper penetration into biological tissues [3–6]. At these depths, the degradation of beam quality through scattering biological tissues can be overcome by a range of wavefront shaping methods [7]. However, these methods are challenging, slow, and are typically single-point correction schemes, requiring rapid recalibration when considering any form of wide-field or volumetric imaging.

Rapid MPM can be achieved with temporal focusing (TF), where the axial localisation is performed by focusing a pulse in time rather than in space [8, 9], alleviating the need for point-scanning with a facile use of a diffracting element. Recently, TF has come to the forefront with the realisation that spectrally dispersed light preserves spatial fidelity throughout scattering media due to the temporal pulse compression being supported only by the in-phase, minimally scattered photons [10–13]. Wide-field

TF MPM has been demonstrated as a novel option for correction-free imaging at a depth of up to seven scattering mean-free-path lengths with two-photon [10] and may go further using three-photon [14] excitation modes. This advance (termed TRAFIX) was enabled with single-pixel detection, wherein structured patterns are sequentially projected onto the sample plane, the total diffuse signal is recorded by a single-pixel detector, and a minimisation algorithm is used to recover the image. This alleviates the need for spatial coherence in the detection path [15], enables compressive sensing [11], and can also be performed in parallel, supporting fast acquisition times [12].

Compressive sensing (CS), in its own right, has led to remarkable achievements [16, 17], with a primary advantage of allowing for sampling well below that required by the Nyquist criterion [18–20]. CS, however, has been applied primarily to macro imaging, with little consideration given to high-resolution microscopy. CS may have a number of advantages in this area, including a reduction in photodamage [21]. CS requires the use of appropriately chosen structured illumination patterns as a measurement basis set. Patterns possessing high spatial frequencies are challenging to relay through microscopy systems due to the diffraction limit, resulting in degraded resolution and fidelity and, ultimately, the loss of information about the sample. In selecting the optimal compression basis, one must consider optimisation of the spatial frequency content, beyond simply using a basis that best suits CS algorithms.

Optimal spatial and frequency sampling has been described by Gabor [22], presenting a trade-off between spatial and frequency localisation that reaches the uncertainty limit. Real-valued Gabor filters (Morlets) have been used to generate a basis for compressive imaging, optimising information transfer to typical frequencies found in photographs [23]. However, this principle is ideally suited for microscopy, where the frequency transfer function is well-known. In this paper, we examine the random Morlet basis (a convolution of a Gabor filter with a random matrix) as an optimal basis set in MPM. We demonstrate that the Morlet basis provides superior performance to the conventional Hadamard and Random bases, with CS and when imaging through scattering media. The elegant formation and optimal performance of the Morlet basis are likely to stimulate its wider adoption for compressive wide-field microscopy.

Pattern efficiency in TRAFIX relies on two principles: the suitability of the basis for CS, and the resilience of the pat-

terned wavefront to propagation and scattering, which we describe in turn. CS is achieved by recognising that most signals are close-to sparse in some domain [20]. Briefly, we consider our linearised image vector \mathbf{x} to comprise a sparse signal \mathbf{s} in some domain, Ψ (here, the discrete cosine transform domain), such that $\mathbf{x} = \Psi\mathbf{s}$. Given that the majority of images are compressible, it is likely that many coefficients of \mathbf{s} are close to zero [20]. Thus, images with N total pixels, can be acquired with $M < N$ measurements, where M exceeds the number of non-zero coefficients of \mathbf{s} . We do this by constructing a measurement basis Φ , comprising M rows of linearised patterns with N columns. Projecting each row sequentially onto the sample generates measurements on the photodetector given by $\mathbf{y} = \Phi\mathbf{x} = \Phi\Psi\mathbf{s} = \Theta\mathbf{s}$. We estimate the image $\hat{\mathbf{x}}$ using l_1 -norm minimisation: $\hat{\mathbf{x}} = \Psi \cdot \arg \min \|\mathbf{s}\|_1, s.t. \Theta\mathbf{s} = \mathbf{y}, i.e.,$ by finding the most sparse \mathbf{s} that can generate the measurements in \mathbf{y} . The efficacy of CS lies in designing Φ such that any linear combination of columns of $\Theta = \Phi\Psi$ are *mutually incoherent* (i.e., possess low correlation between any two columns) [24]. Orthonormal bases, such as the Hadamard, perform well when fully sampled ($M = N$); however, when under-sampled ($M < N$), lead to a Θ that is *not* mutually incoherent. Interestingly, random matrices are mutually incoherent and, as such, can be used for a substantially higher compression [20].

For high-resolution applications, patterns to be imaged into the sample space are susceptible to degradation arising from spatial filtering in the objective's back focal plane. Conventional CS patterns, such as the random pattern, possess very broad spatial frequency spectra. This leads to the loss of high-frequency components in both illumination and detection, a discrepancy between the generated and the projected Ψ , and thus the loss of image quality. The proposed random Morlet patterns can be contained primarily within the entrance pupil of the objective, thus, they will be transmitted faithfully.

The Morlet wavelet is described by a real-valued, centred, zero-mean Gabor filter:

$$g(x, y) = N \cdot \exp \left\{ -\frac{x^2 + y^2}{2\sigma^2} \right\} \times \cos \left\{ \frac{\pi n_p}{2\sigma} [x \cos \theta + y \sin \theta] \right\}, \quad (1)$$

where the first exponential term is a Gaussian with a given space-frequency bandwidth, σ , and the second term sets a modulation along a given direction θ that shifts the wavelet in the frequency domain; n_p is the number of peaks of the Morlet wavelet; and, N in a normalisation factor, chosen such that $|g| = 1$.

A basis is generated from a set of Morlet wavelets with σ and n_p chosen randomly from a normal distribution, convolved with an array of normally distributed random values [23]. The resultant basis, inspired by Gabor's filters [22], allows for fine spatial features to be sampled, whilst minimising the required spatial frequency bandwidth required. In particular, it is important to confine the frequency content of the basis to that supported by the imaging system. For a Morlet pattern illuminating the sample, we can approximate its field in the Fourier plane as the Fourier transform of $g(x, y)$ evaluated at spatial frequencies $(x_2/\lambda f, y_2/\lambda f)$. A Morlet wavelet in the Fourier plane is described by:

$$G(x_2, y_2) \propto \exp \left\{ -\frac{1}{2\sigma_f^2} \left[(x_2 - a_f \cos \theta)^2 + (y_2 - a_f \sin \theta)^2 \right] \right\}, \quad (2)$$

where: $\sigma_f = f\lambda/2\pi\sigma$ and $a_f = f\lambda n_p/4\sigma$ represent the frequency bandwidth and the frequency shift, respectively. Given a particular back aperture radius, $R = f \cdot \text{NA}$, it is trivial to select σ and n_p that fit, for instance, $a_f + 2\sigma_f < R$. By contrast, a binary Random basis will uniformly overfill the back aperture to the Nyquist spatial frequency.

Fig. 1 illustrates the experimental set-up of TRAFIX, where a pulsed laser source (Chameleon Ultra II, Coherent) illuminates a digital micromirror device (DMD; DLP9000, TI). The laser is tuned to a central wavelength of 800-nm, with a 140-fs pulse duration and an 80-MHz repetition rate. The DMD is imaged onto a blazed reflective diffraction grating (DG; 600 lines/mm, Thorlabs), which spatially disperses the light in the back aperture of the objective. The dispersed pulse is spatio-temporally refocused in the sample plane by a lens (L; $f=400$ mm) and an air immersion objective (20 \times , 0.75 NA, Nikon). The axial resolution is approximately 7 μm in the absence of scattering media [10]. The multiphoton signal is diffusely collected by a photomultiplier tube (PMT; PMT2101, Thorlabs). In-house built MATLAB and C# software is used to generate the basis, and sequentially project it on the DMD and record the PMT signal. CS using l_1 -norm minimisation is performed using the open source 'l₁-magic' toolbox [18] and approximated using the 'NESTA' algorithm [25].

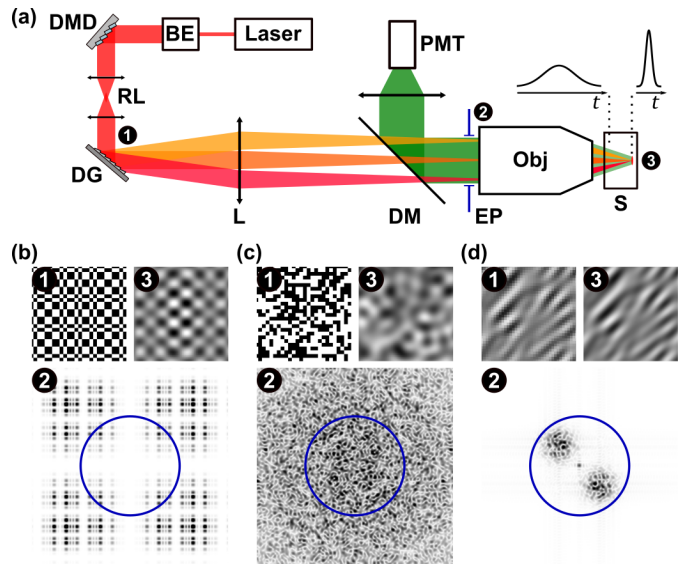


Fig. 1. Principle of TRAFIX. (a) Optical set-up. BE: beam expander; DMD: digital micromirror device; RL: relay lenses; DG: diffraction grating; L: lens; DM: dichroic mirror; EP: entrance pupil; Obj: objective; S: sample; and, PMT: photomultiplier tube. Numbered locations correspond to (1) the image on the DG, (2) the Fourier plane of the Obj, and (3) the sample image plane. (b-d) Simulated field intensity in free space of a Hadamard, Random and Morlet pattern, respectively, at locations (1-3). Clipping by the EP is illustrated by a blue circle.

Fig. 1(b-d) illustrates representative patterns from Hadamard, Random and Morlet bases, respectively, evaluated using Fourier optics in free space. The pixel size was chosen to Nyquist sample the diffraction limit (~ 500 nm). A pattern is shaped by the DMD (location (1)), and a Fourier plane (FP) is formed by lens, L, at the back focal plane of the objective (location (2)) (DC component omitted for clarity). The periodic structure of the Hadamard pattern in Fig. 1(b) leads to a broad structured field intensity in

the FP, whilst the Random pattern in Fig. 1(c) leads to a speckle pattern in the FP. It is evident that both patterns overflow the entrance pupil of the objective, which is marked by the blue circle (15-mm diameter). This leads to a substantial portion of the field being filtered out by the aperture before reaching the sample. Thus, the patterns look considerably distorted at the sample image plane (location (3)). Patterns with a pixel size exceeding the diffraction limit can be transmitted, however, they would sub-sample the Nyquist frequency twofold. Fig. 1(c) illustrates that the Morlet field at the FP can be effectively transmitted through the objective, leading to the image plane at the sample and the DG being nearly identical.

We experimentally evaluate the bases on 4.8- μm green fluorescent polystyrene beads (G0500, Thermo Scientific). The beads were suspended in water, dried onto a cover slip and sealed using UV-curing optical adhesive (68, Norland), minimising photobleaching to less than 5% in 2 hours of continuous imaging. Fig. 2(a-c) shows the beads imaged with 64×64 -pixel bases (4096 patterns) over a 45- μm field-of-view with various levels of compression, compared to a reference image taken by an EMCCD camera (iXon^{EM}+ 885, Andor) (Fig. 2(d)). The illumination intensity and PMT integration time were constant for all recordings; thus, the images are scaled to the same noise floor. Image quality is quantified as the peak signal-to-noise ratio (PSNR) (Fig. 2(e)), defined as: $10 \log_{10}(\max(I)^2/MSE)$, where I is the image intensity and MSE is the mean squared error between the image and the camera reference. Qualitatively, and from the PSNR, we can see that the Hadamard basis performs well without compression; however, image fidelity declines rapidly with compression. Even at 25% compression (*i.e.*, using 3/4 of the total patterns), image quality drops more than twofold. The Random basis performs consistently with compression; however, since it comprises the highest spatial frequency bandwidth of all bases, the maximum achievable PSNR is reduced overall. The most significant benefit is observed using the Morlet basis, demonstrating the highest PSNR and a high resilience of image quality to compression. Remarkably, even at 87.5% compression, individual beads can be resolved and localised, with a dynamic range above the Hadamard and Random bases at 25% compression. We note that since the Random and Morlet bases are not orthonormal, CS recovery at no to low compression leads to an overdetermined measurement matrix whose inverse is ill-conditioned. To overcome this, the no-compression acquisitions Figs. 2(b-1) and (c-1) are decomposed into two 50% compression datasets, which are averaged together.

We further evaluate the capacity of these bases to image through scattering media. Fig. 3 shows 4.8- μm beads imaged through a 360- μm thick scattering phantom (mean-free-path length, $l_s = 115 \mu\text{m}$), described in [10]. At this thickness, multiple scattering of the two-photon signal scrambles spatial information such that no discernible image can be formed at the camera. However, using single-pixel detection alleviates the need to preserve spatial information, thus, beads can still be resolved (Figs. 3(a-d)). Since the phantom is not perfectly flat, not all beads are in the focal plane. Fig. 3(d) visualises the intensity across a bead in focus for all bases. We quantify image quality as the contrast-to-noise ratio (CNR), calculated as the difference in the mean intensity of the bead and the background, over the standard deviation of the background noise, *i.e.*, $CNR = (\bar{I}_{bead} - \bar{I}_{bg})/\sigma_{bg}$. With no compression, Hadamard, Random and Morlet bases generate a CNR of 6.5, 10 and 13, respectively. Unlike the PSNR in Fig. 2(e), the Hadamard performs poorly. In Fig. 3(a), we can see that the Hadamard basis gener-

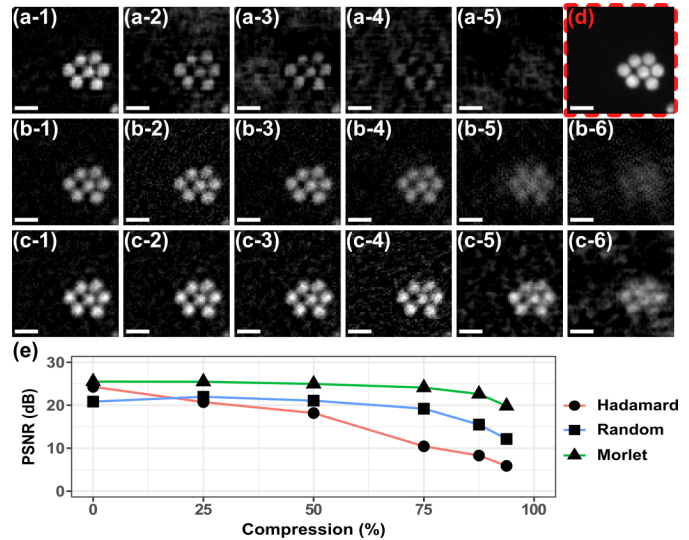


Fig. 2. TRAFIX images of 4.8- μm beads using 64×64 -pixel (a) Hadamard, (b) Random and (c) Morlet bases, with 0, 25, 50, 75, 87.5 and 93.75% compression marked by labels (1-6), respectively. The red-outlined inset (d) is a reference camera image. The scale bars are 10 μm . (e) Image quality (PSNR) as a function of compression.

ates a non-uniform point-spread function (PSF). The periodic nature of the Hadamard basis may lead to a discrete proportion of the patterns being either transmitted or lost. In Fig. 3(a), this is manifested as larger scale pixelation. Interestingly, with 87.5% compression, no discernible image can be reconstructed from the Hadamard, and the CNR becomes 0.2, 4.9 and 9.8, for each respective basis. It is evident that the Morlet basis generates superior image quality, with and without compression through scattering. Fig. 3(h) demonstrates that even at high compression and through scattering, the bead is clearly identified.

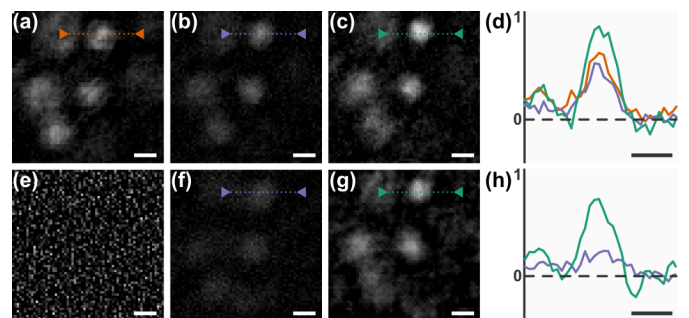


Fig. 3. TRAFIX images of 4.8- μm beads through 360 μm of a scattering phantom, with (a-d) no compression and (e-h) 87.5% compression; using 64×64 -pixel (a,e) Hadamard, (b,f) Random and (c,g) Morlet bases, with corresponding (d,h) line plots from the regions indicated by the colored dashed lines. (e) is omitted in (h) for clarity. The scale bars are 5 μm .

A particular advantage of CS in MPM is that the use of fewer patterns minimises photobleaching, which is an important consideration for sensitive markers, for *in vivo*, and for long-term imaging applications. Whilst the illumination profiles are different for each basis, the mean irradiance of each pattern is equivalent. We have now measured photobleaching of 64×64 -

pixel bases on a uniform film of super-yellow polymer. The rate of photobleaching was the same for each basis to within a 6% error. If the time of exposure is limited, the Morlet basis should permit the highest sampling resolution for a given image quality. Fig. 4 demonstrates this by imaging 10- μm beads without scattering over a 220- μm field-of-view with a constrained acquisition of 3072 patterns. Equivalent PSNR (Fig. 2(e)) is obtained from Hadamard, Random and Morlet bases with 25%, 67% and 82%, respectively. Within these limits, we can employ 64-, 96- and 128-pixel wide bases, respectively. Given the larger sampling, we employ the substantially more efficient NESTA algorithm [25] that approximates the l_1 -minimisation problem, whilst adhering to a set spatial smoothness, $\|y - \Phi x\|_{l_2} < \epsilon$. Figs. 4(d–f) show a close up of the beads. It is evident that there is a progressive increase in the sampling resolutions, with the Morlet basis clearly delineating beads with the least pixelation.

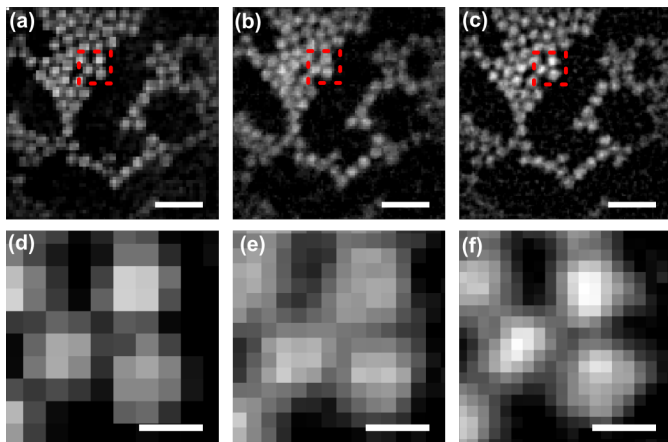


Fig. 4. TRAFIX images of 10- μm beads without scattering over a 220- μm field-of-view using 3072 patterns (equal acquisition time). (a) 64 \times 64-pixel Hadamard, (b) 96 \times 96-pixel Random, (c) 128 \times 128-pixel Morlet bases, corresponding to 25%, 67% and 82% compression. (d,e,f) are the respective magnified insets of (a,b,c), marked by the red-dashed square. The scale bars are 50 μm for (a,b,c) and 10 μm for (d,e,f).

In this paper, we have demonstrated that the random Morlet basis presents an elegant and optimal solution to compressive imaging in microscopy. CS is central to the recent flurry of demonstrations that combined wide-field temporal focusing with pattern illumination to achieve correction-free multiphoton imaging at improved depths [10–12, 14]. We have demonstrated that unlike many other conventional CS applications, a substantial consideration must be given to the fidelity of the measurement basis as it is relayed through the focusing system and scattered by the sample.

The Morlet basis, designed to optimise wavefront propagation through a microscopy system, likely leads to an overall superior performance in image quality and a higher resilience to compression. Whilst we have demonstrated this for samples of beads, a more in depth study of the performance of the Morlet basis in biological samples would be valuable. Furthermore, the Morlet basis minimises power loss, which is important to MPM, where high illumination power is difficult to achieve over a wide field-of-view with affordable laser sources. The high compression achievable with the Morlet basis results in a substantial reduction in illumination time and, thus, a likely reduction in photodamage [21]. A further study of photobleach-

ing in biological samples would be instructive, as photodamage is a particular area of concern for two-photon and latterly three-photon microscopy. In this area, as well as due to its optimal performance, the Morlet basis is well-positioned to make a considerable impact for compressive wide-field single-pixel multiphoton imaging.

Acknowledgements We thank the UK Engineering and Physical Sciences Research Council (grant EP/P030017/1) and the European Union’s Horizon 2020 Framework Programme (H2020) (675512, BE-OPTICAL). We thank Vanya Metodieva, Wardiya Afshar Saber and Federico M. Gasparoli for helpful discussions and support. The research data underpinning this publication can be accessed at <https://doi.org/10.17630/8a54533e-c4ce-40d0-befe-401ddb9daadb>.

REFERENCES

- N. Ji, J. Freeman, and S. L. Smith, *Nat. Neurosci.* **19**, 1154 (2016).
- H. Tu, Y. Liu, D. Turchinovich, M. Marjanovic, J. K. Lyngsø, J. Lægsgaard, E. J. Chaney, Y. Zhao, S. You, W. L. Wilson, B. Xu, M. Dantus, and S. A. Boppart, *Nat. Photonics* **10**, 534 (2016).
- A. Escobet-Montalbán, F. M. Gasparoli, J. Nytk, P. Liu, Z. Yang, and K. Dholakia, *Opt. Lett.* **43**, 5484 (2018).
- T. Wang, D. G. Ouzounov, C. Wu, N. G. Horton, B. Zhang, C.-H. Wu, Y. Zhang, M. J. Schnitzer, and C. Xu, *Nat. Methods* **15**, 789 (2018).
- O. A. Shemesh, D. Tanese, V. Zampini, C. Linghu, K. Piatkevich, E. Ronzitti, E. Papagiakoumou, E. S. Boyden, and V. Emiliani, *Nat. Neurosci.* **20**, 1796 (2017).
- S. Weisenburger, F. Tejera, J. Demas, B. Chen, J. Manley, F. T. Sparks, F. M. Traub, T. Daigle, H. Zeng, A. Losonczy, and A. Vaziri, *Cell* **177**, 1050 (2019).
- N. Ji, *Nat. Methods* **14**, 374 (2017).
- G. Zhu, J. v. Howe, M. Durst, W. Zipfel, and C. Xu, *Opt. Express* **13**, 2153 (2005).
- D. Oron, E. Tal, and Y. Silberberg, *Opt. Express* **13**, 1468 (2005).
- A. Escobet-Montalbán, R. Spesyvtsev, M. Chen, W. A. Saber, M. Andrews, C. S. Herrington, M. Mazilu, and K. Dholakia, *Sci. Adv.* **4**, eaau1338 (2018).
- M. Alemohammad, J. Shin, D. N. Tran, J. R. Stroud, S. P. Chin, T. D. Tran, and M. A. Foster, *Opt. Lett.* **43**, 2989 (2018).
- D. N. Wadduwage, J. K. Park, J. R. Boivin, Y. Xue, and P. T. C. So, *arXiv:1902.10737 [physics]* (2019).
- E. Papagiakoumou, A. Bégue, B. Leshem, O. Schwartz, B. M. Stell, J. Bradley, D. Oron, and V. Emiliani, *Nat. Photonics* **7**, 274 (2013).
- A. Escobet-Montalbán, P. Wijesinghe, M. Chen, and K. Dholakia, *Multiphoton Microscopy in the Biomedical Sciences XIX*, (SPIE BiOS, 2019), p. 108821G.
- V. Durán, F. Soldevila, E. Irlés, P. Clemente, E. Tajahuerce, P. Andrés, and J. Lancis, *Opt. Express* **23**, 14424 (2015).
- J. H. Shapiro, *Phys. Rev. A* **78**, 061802 (2008).
- M.-J. Sun, M. P. Edgar, G. M. Gibson, B. Sun, N. Radwell, R. Lamb, and M. J. Padgett, *Nat. Commun.* **7**, 12010 (2016).
- E. J. Candes, J. Romberg, and T. Tao, *IEEE Transactions on Inf. Theory* **52**, 489 (2006).
- D. L. Donoho, *IEEE Trans. Inf. Theor.* **52**, 1289 (2006).
- R. G. Baraniuk, *IEEE Signal Process. Mag.* **24**, 118 (2007).
- M. Wroninger, X. Darzacq, C. Zimmer, and M. Mir, *Opt. Express* **25**, 13668 (2017).
- D. Gabor, *J. Inst. Electr. Eng. - Part III: Radio Commun. Eng.* **93**, 429 (1946).
- K. M. Czajkowski, A. Pastuszczak, and R. Kotyński, *Sci. Reports* **8**, 466 (2018).
- E. J. Candes, J. Romberg, and T. Tao, *Commun. on Pure Appl. Math.* **59**, 1207 (2006).
- S. Becker, J. Bobin, and E. Candès, *SIAM J. on Imaging Sci.* **4**, 1 (2011).